Supporting Information for: **A point-of-need framework for illicit drug identification with high-resolution mass spectrometry**

Thomas P. Forbes[1*], Elizabeth L. Robinson[1], Edward Sisco[1], and Abigail Koss[2]

[1]*National Institute of Standards and Technology, Materials Measurement Science Division, Gaithersburg, Maryland 20899, USA*

[2]*TOFWERK USA, Boulder, Colorado 80301, USA*

[*] Corresponding author: TPF: *E-mail: thomas.forbes@nist.gov*

Supporting Information Table of Contents

Data Availability

Raw data files, extracted mass spectra, and derived data files are available on the NIST Public Data Repository: *https://doi.org/10.18434/mds2-3591*.

Supplemental Methods

Supplemental Tables and Figures

Supplemental Methods

Ionization Pathways. In general, chemical ionization through VUV and dopant adduct formation was achieved by targeting specific adducts. For example, iodide adducts were readily formed in negative mode operation with VUV and an iodine permeation tube. Alternatively, ammonium adducts are a common choice for positive mode operation and have been demonstrated with similar ion sources such as DART. However, we targeted protonation to simplify spectral interpretation and employ existing libraries (*e.g.,* the NIST DART Forensics Mass Spectral Library). Similarly, the DBDI source generated significant nitrate in negative mode operation, but predominantly generated protonation in positive ionization mode.

Acetone-assisted VUV photoionization was a combination charge exchange or proton transfer with ionized dopant (acetone) species (S. Wang *et al*., https://doi.org/10.1021/acs.analchem.8b04168)[1] and adduct formation. Related charge exchange and protonation reaction often incorporate ambient water molecules. Acetone properties from the literature and NIST Chemistry WebBook (https://webbook.nist.gov/chemistry/) include ionization energy: 9.7 eV, proton affinity: 812.0 kJ/mol, photoionization cross section: 5.1×10^{-18} cm^2, and vapor pressure: 30.78 kPa. Equations (S1)-(S3) represent the reactions for acetone (C_3H_6O) photoionization:

$$C_3H_6O + h\nu \rightarrow C_3H_6O^{+\cdot} + e^- \quad \text{(S1)}$$

$$C_3H_6O^{+\cdot} + H_2O \rightarrow (C_3H_6O + H)^+ + OH^{\cdot} \quad \text{(S2)}$$

$$(C_3H_6O + H)^+ + C_3H_6O \rightarrow [(C_3H_6O)_2 + H]^+ \quad \text{(S3)}$$

Proton transfer reactions (Equation (S4)) and adduct formation (Equation (S5)) between ionized acetone species and the analyte likely dominated analyte ionization. Given the relative ionization energies and proton affinities of acetone vs most organic drug molecules, the proton transfer

reaction (Equation(S4)) was likely more efficient. Here, *M*, represents a potential analyte (*e.g.,* drug molecule):

$$[(C_3H_6O)_2 + H]^+ + M \rightarrow (M + H)^+ + (C_3H_6O)_2 \quad \text{(S4)}$$

$$(C_3H_6O + H)^+ + M \rightarrow [M + C_3H_6O + H]^+ \quad \text{(S5)}$$

The in-line DBDI ionization has been studied extensively in the literature and combines a number of traditional ionization pathways (J.-C. Wolf *et al.,* https://doi.org/10.1007/s13361-016-1420-2 and M. Weber *et al*., https://doi.org/10.1021/jasms.2c00279).[2, 3] These pathways involve similar charge exchange and proton transfer reactions as above; however, the reaction series originates with electron ionization from the plasma. The plasma generates excited water, gas (*e.g.,* N_2), and analyte species:

$$H_2O + e^- \rightarrow H_2O^{+\cdot} + 2e^- \quad \text{(S6)}$$

$$N_2 + e^- \rightarrow N_2^{+\cdot} + 2e^- \quad \text{(S7)}$$

$$M + e^- \rightarrow M^{+\cdot} + 2e^- \quad \text{(S8)}$$

Similarly, the excited N_2 may interact with water or analyte molecules through charge exchange:

$$N_2^{+\cdot} + H_2O \rightarrow H_2O^{+\cdot} + N_2 \quad \text{(S9)}$$

$$M + N_2^{+\cdot} \rightarrow M^{+\cdot} + N_2 \quad \text{(S10)}$$

Subsequent proton transfer reactions with water yield protonated analyte species:

$$M^{+\cdot} + H_2O \rightarrow (M + H)^+ + OH^{\cdot} \quad \text{(S11)}$$

Or:

$$H_2O^{+\cdot} + H_2O \rightarrow (H_2O + H)^+ + OH^{\cdot} \quad \text{(S12)}$$

$$(H_2O + H)^+ + M \rightarrow (M + H)^+ + H_2O \quad \text{(S13)}$$

The configuration presented here also includes charge exchange and proton transfer reactions with residual acetone molecules leaking from the unused permeation tube, adding reactions (S1)-(S2) and (S4)-(S5) to potential pathways.

Supplemental Tables and Figures

Table S1. Demonstrated calibration with three acetone peaks (protonated monomer, protonated monomer-water adduct, and protonated dimer). Data collected with the acetone-VUV configuration.

Compound	**$[M+H]^+$ *(m/z)***	**Single-Component Analytes**			**15-Component Mixture**		
		Observed	***Δm/z***	**ppm**	**Observed**	***Δm/z***	**ppm**
Methamphetamine	150.1283	150.1313	0.0030	20.27	150.1317	0.0035	23.01
α-PBP	218.1545	218.1596	0.0051	23.53	218.1647	0.0102	46.61
Tenocyclidine	250.1629	250.1739	0.0110	43.87	250.1759	0.01300	51.79
Cocaine	304.1549	304.1722	0.0174	57.07	304.1741	0.0193	63.29
Furanyl Fentanyl	375.2073	375.2321	0.0248	66.10	375.2345	0.0273	72.69

Table S2. Demonstrated calibration with PEG-600 calibrant and three acetone peaks. Data collected with the acetone-VUV configuration.

Compound	**$[M+H]^+$ *(m/z)***	**Single-Component Analytes**			**15-Component Mixture**		
		Observed	***Δm/z***	**ppm**	**Observed**	***Δm/z***	**ppm**
Methamphetamine	150.1283	150.1281	-0.0002	-1.17	150.1289	0.0007	4.32
α-PBP	218.1545	218.1539	-0.0005	-2.49	218.1581	0.0037	16.75
Tenocyclidine	250.1629	250.1658	0.0029	11.60	250.1681	0.0052	20.63
Cocaine	304.1549	304.1612	0.0063	20.64	304.1629	0.0080	26.26
Furanyl Fentanyl	375.2073	375.2169	0.0097	25.76	375.2187	0.0115	30.56

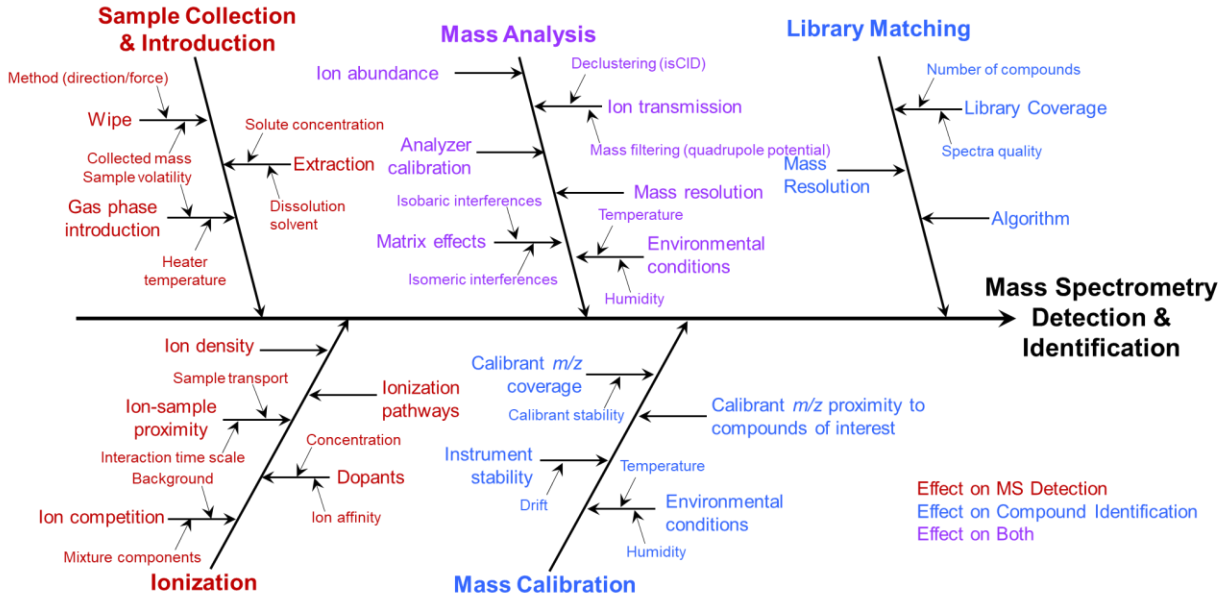

Figure S1. Cause-and-effect analysis using an Ishikawa diagram to layout and identify components impacting variability or uncertainty in two main results – compound detection and compound identification.

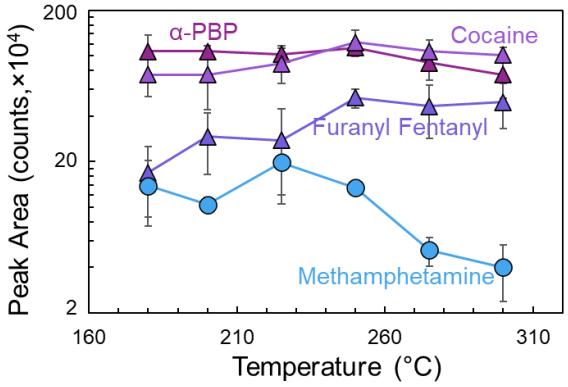

Figure S2. MS response (*i.e.*, peak areas) as a function of increasing thermal desorption temperature for select drugs. Sample was a glass melting point capillary dipped in a 5 ng/µL (of each component) 15-component drug mixture. DBDI source was run at 1300 V and 15 kHz. Data and uncertainty display the average and standard deviation of seven (*n*=*7*) replicate measurements.

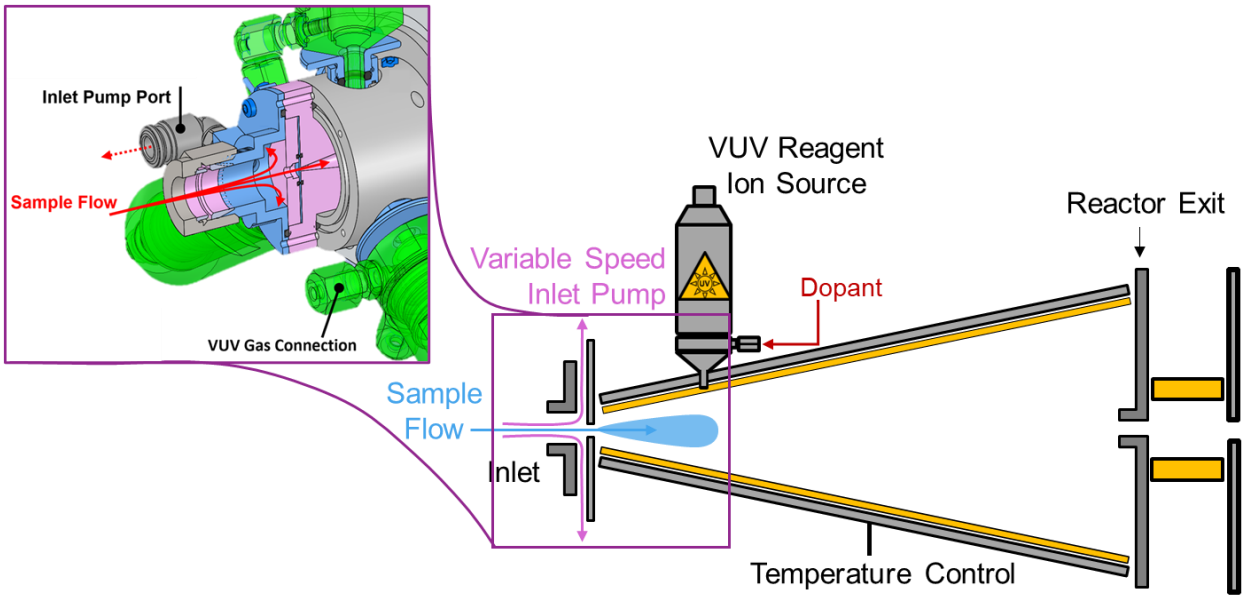

Figure S3. Schematic representation of the mass spectrometer inlet and reaction chamber upstream of the first quadrupole ion guide. Sample flow was entrained through the inlet by instrument vacuum system and a supporting variable speed inlet pump. Inset: 3D model of inlet displaying sample and pump flow. (Schematics adapted from TOFWERK)[4]

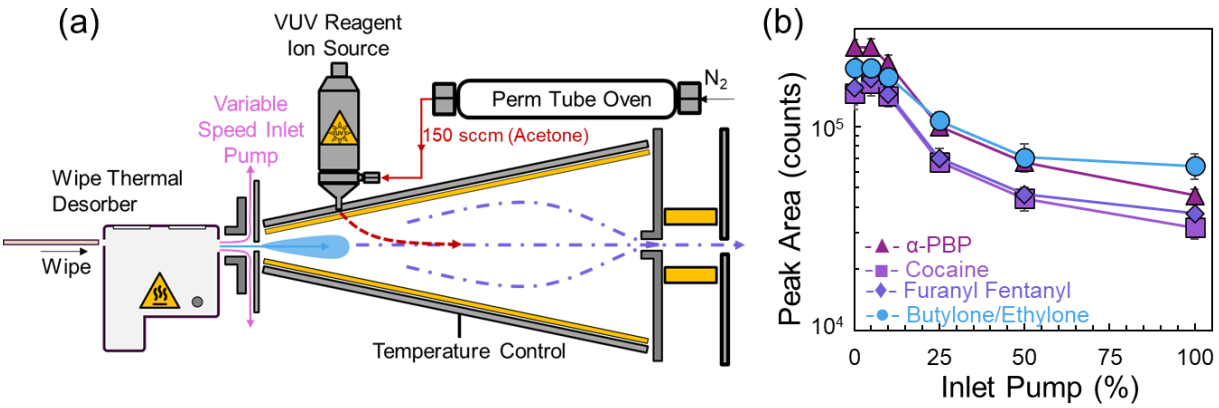

Figure S4. (a) Schematic representation of the wipe-based thermal desorber coupled with the acetone-VUV photoionization platform. (b) Peak areas of 5 ng (of each component) deposits of 15-component mixture as a function of inlet pump flow. Parameters: TD: 225 °C, ion-molecule reactor temp: 50°C, perm tube flow: 100 cm^3/min, VUV voltage: 1600 V. Data points and uncertainty represented by average and standard deviation of 4-5 replicate measurements.

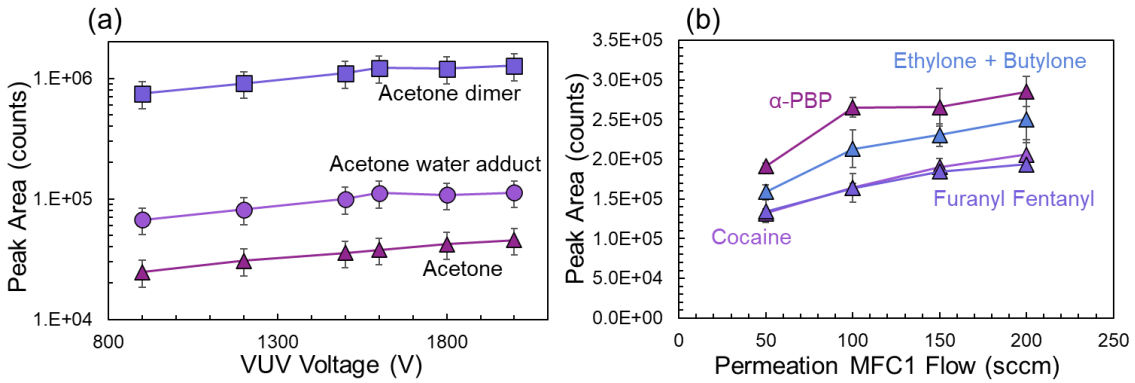

Figure S5. MS response (*i.e.,* peak areas) for (a) acetone-related ions and (b) protonated drug ions as a function of VUV voltage and acetone flow rate, respectively. Acetone-assisted VUV photoionization of 5 ng/µL 15-component drug mixture – (a) TD: 250°C, ion-molecule reactor temperature: 50°C, permeation tube flow: 150 sccm, VUV: variable, inlet pump: 5 % and (b) TD: 225°C, reactor temperature: 50°C, permeation tube flow: variable, VUV: 1600 V, inlet pump: 5 %. Data and uncertainty display the average and standard deviation of five (*n=5*) replicate measurements.

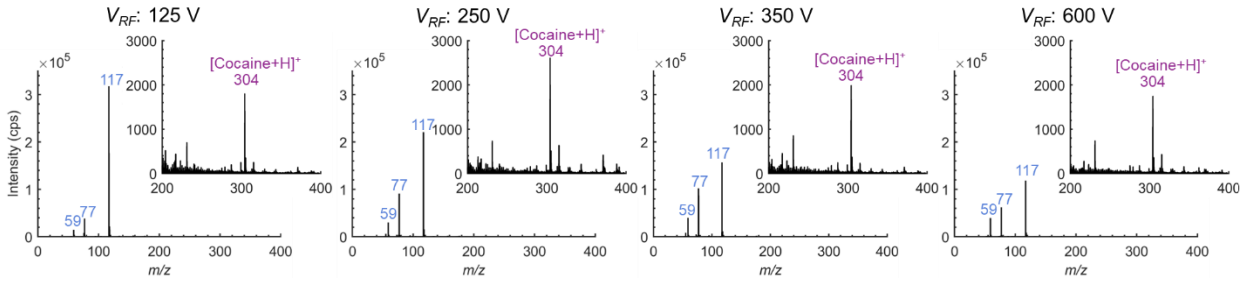

Figure S6. Representative mass spectra of the background acetone-related ion distribution and protonated cocaine (insets) as a function of increasing *RF* potential on the first ion guide quadrupole. Acetone-assisted VUV photoionization of 5 ng/µL cocaine solution – TD: 250°C, ion-molecule reactor temperature: 50°C, permeation tube flow: 150 sccm, VUV: 1600 V, inlet pump: 5 %.

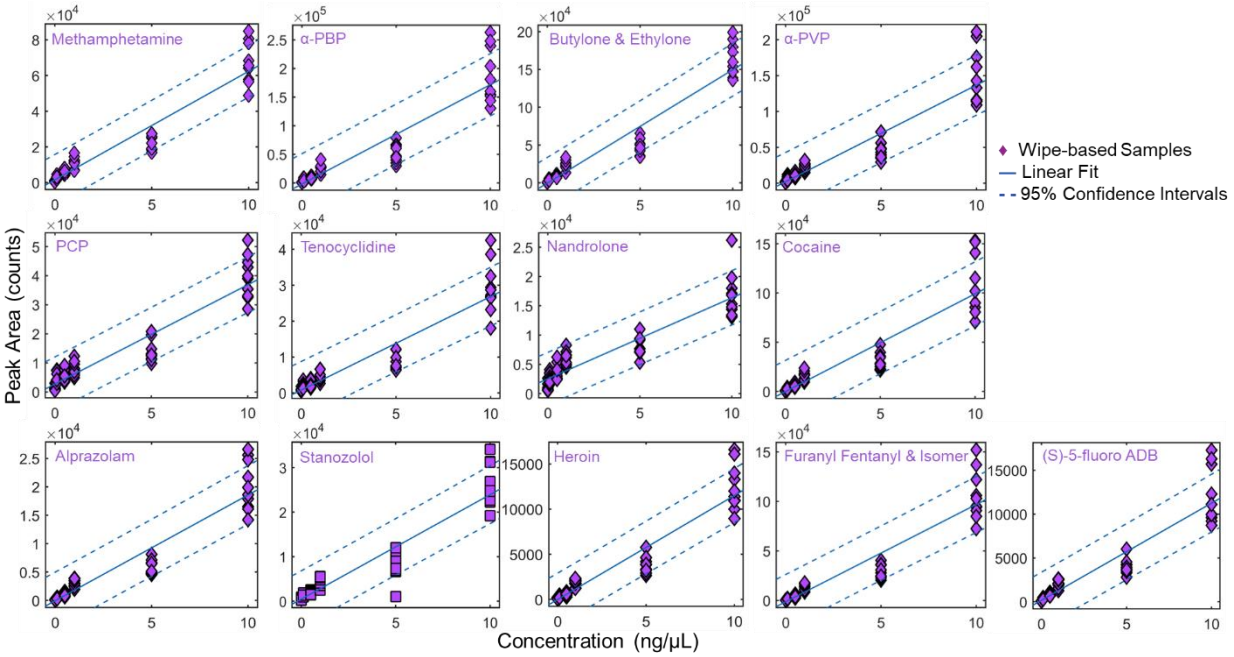

Figure S7. Response curves for the 15-component drug mixture at (0, 0.1, 0.5, 1, 5, 10) ng/μL with acetone-assisted VUV photoionization - TD: 250°C, reactor temperature: 50°C, permeation tube flow: 150 sccm, VUV: 1600 V, inlet pump: 5 %. Ten (*n=10*) replicate measurements at each concentration level.

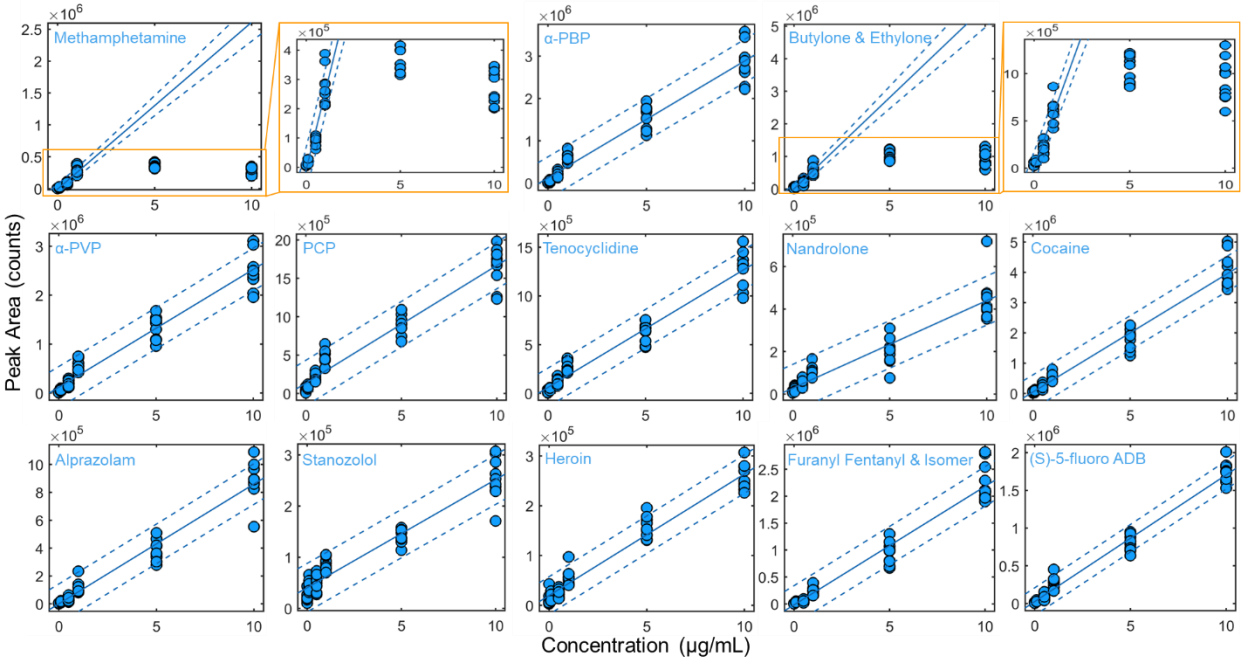

Figure S8. Response curves for the 15-component drug mixture at (0, 0.1, 0.5, 1, 5, 10) ng/μL with DBDI ionization - TD: 250°C, DBDI voltage: 1400 V, DBDI frequency: 15 kHz, inlet pump: 25 %. Ten (*n=10*) replicate measurements at each concentration level.

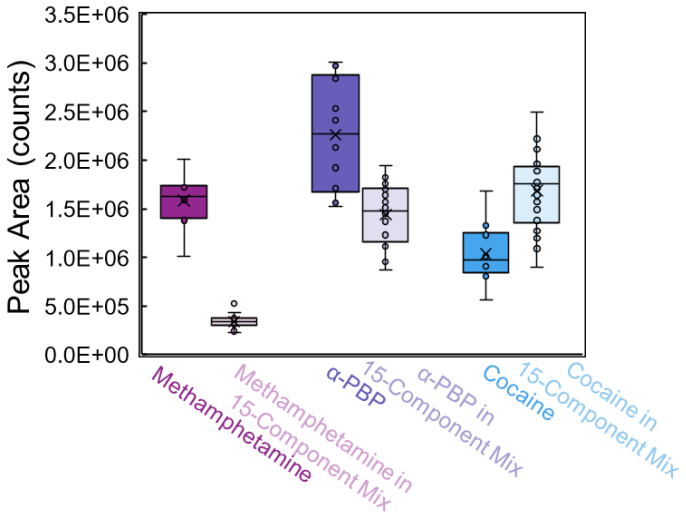

Figure S9. Replicate peak area measurements of methamphetamine, α-PBP, and cocaine in single-component solutions (dark boxes) and in the 15-component mixture – 1:15 mass ratio (light boxes). DBDI ionization of 5 ng/µL solutions - TD: 250°C, DBDI voltage: 1400 V, DBDI frequency: 15 kHz, inlet pump: 25 %.

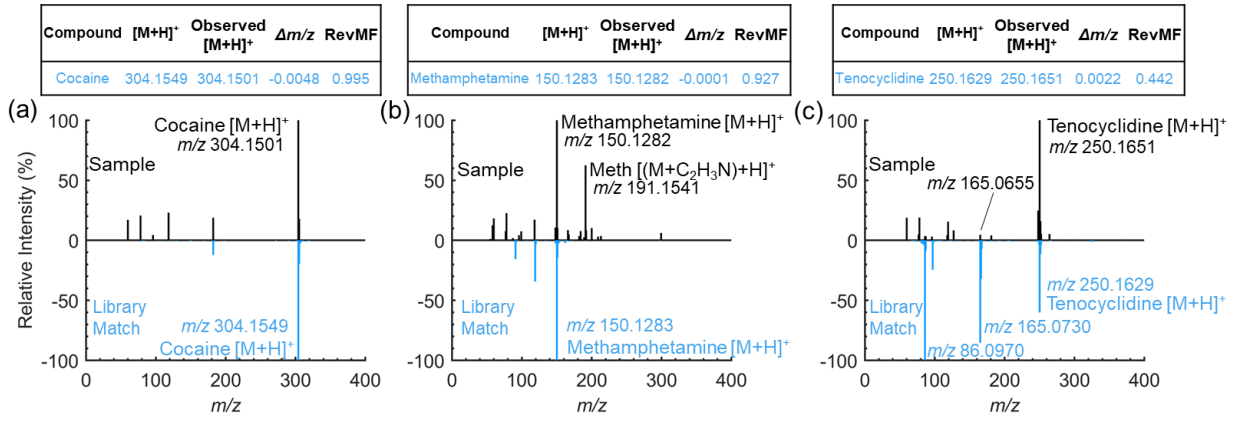

Figure S10. Single-spectrum matching (*i.e.,* low fragmentation) of (a) cocaine, (b) methamphetamine, and (c) tenocyclidine ionized by DBDI (TD: 250°C, DBDI voltage: 1400 V, DBDI frequency: 15 kHz, inlet pump: 25 %) and matched using the DIT with the NIST DART-MS Forensics Database library. DIT search results and match factor displayed in insets.

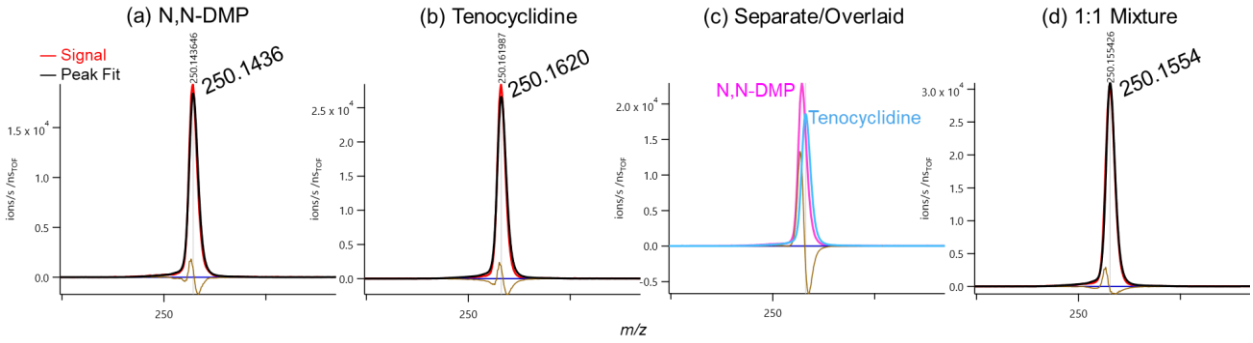

Figure S11. Mass spectra in the region of *m/z* 250 for (a) neat N,N-DMP, (b) neat Tenocyclidine, (b) the separate spectra overlaid, and (d) a 1:1 mixture of the two.

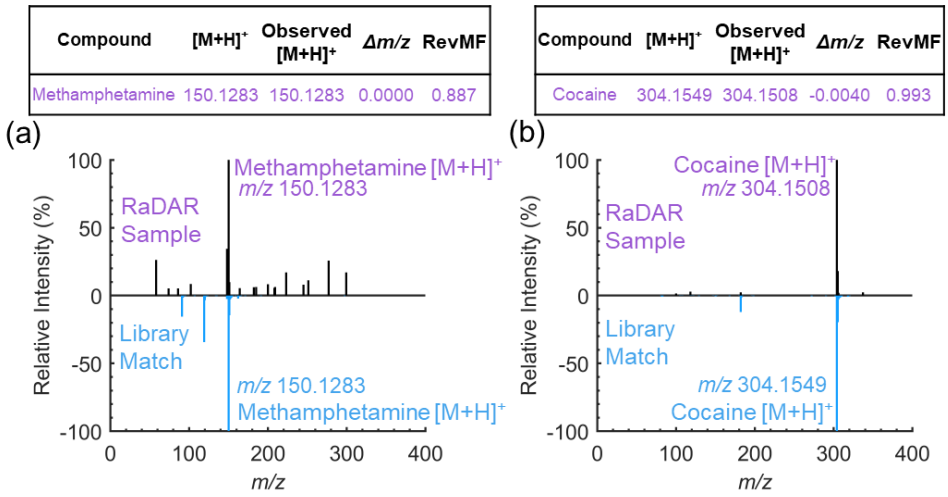

Figure S12. Low fragmentation DBDI-MS mass spectra of RaDAR samples (a) #1 and (b) #2 with matched compounds labeled. Insets display search results and match scores from the DIT. Parameters: TD: 250°C, DBDI voltage: 1400 V, DBDI frequency: 15 kHz, inlet pump: 25 %.

Compound	[M+H]⁺	Observed [M+H]⁺	Δm/z	RevMF
Mannitol	183.0869	183.0855	-0.0014	0.533

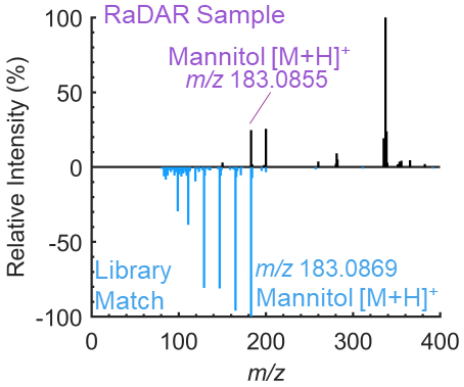

Figure S13. Low fragmentation DBDI-MS mass spectra of RaDAR sample 19181 with only the mannitol match peaks labeled. Inset displays search results and match scores from the DIT. Parameters: TD: 250°C, DBDI voltage: 1400 V, DBDI frequency: 15 kHz, inlet pump: 25 %.

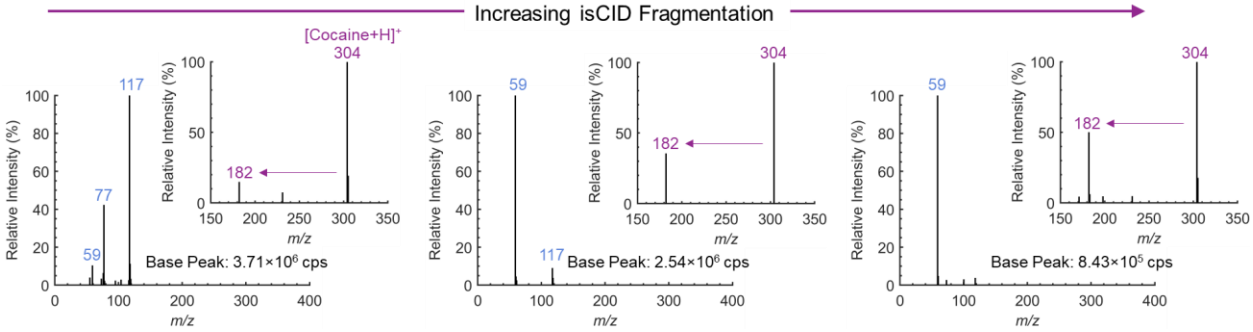

Figure S14. Acetone ion distribution as a function of increasing isCID fragmentation with solid rod quadrupole 1. Insets display cocaine fragmentation. Voltages: nozzle/reactor exit, quad bias, skimmer (0, 0, -1) V, (0, 8, 10) V, and (4, 14, 18) V. Further increasing of isCID voltages with this configuration greatly diminished quadrupole transmission. Source parameters: TD: 250°C, DBDI voltage: 1400 V, DBDI frequency: 15 kHz, inlet pump: 25 %.

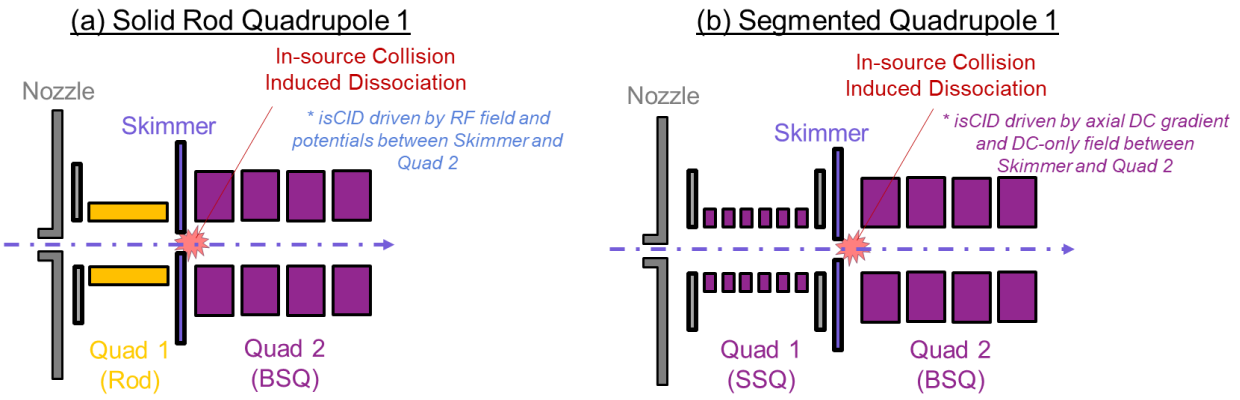

Figure S15. Simplified schematics of the isCID regions for (a) the solid rod quadrupole 1 hardware (with Aim reactor) and (b) the short segmented quadrupole (SSQ) 1 hardware (with aerodynamic-assist interface).

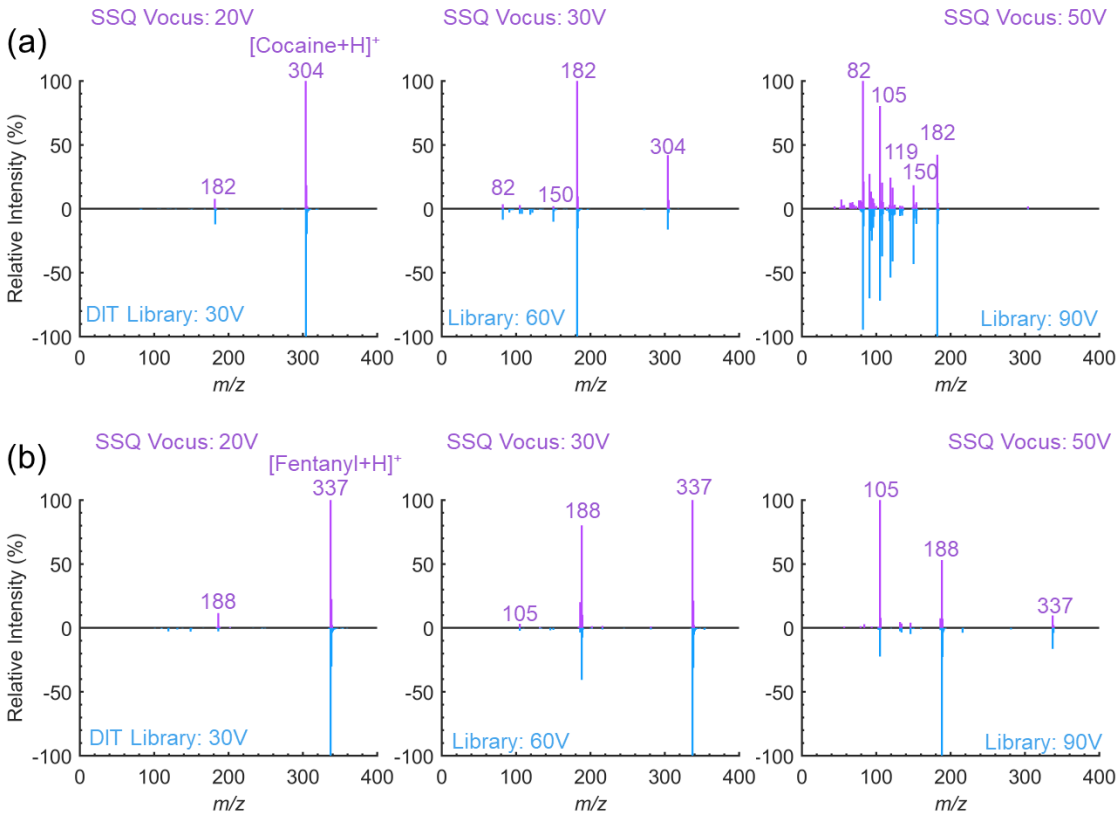

Figure S16. Comparison of (a) cocaine and (b) fentanyl mass spectra at a series of increasing isCID fragmentation voltages (20 V, 30 V, 50 V) to the NIST DART-MS Forensics Database spectra (30 V, 60 V, 90 V) with the SSQ and aerodynamic-assist interface hardware (Aim reactor and solid rod quadrupole removed).
isCID 20V: entrance potential: 9.0 V, SSQ front: 8.0 V, SSQ back: 22.7 V, lens skimmer: 21.7 V
isCID 30V: entrance potential: 9.0 V, SSQ front: 7.9 V, SSQ back: 34.7 V, lens skimmer: 31.5 V
isCID 50V: entrance potential: 20 V, SSQ front: 25 V, SSQ back: 54.7 V, lens skimmer: 51.5 V

References

(1) Wang, S.; Wang, W.; Li, H.; Xing, Y.; Hou, K.; Li, H. Rapid On-Site Detection of Illegal Drugs in Complex Matrix by Thermal Desorption Acetone-Assisted Photoionization Miniature Ion Trap Mass Spectrometer. *Anal.Chem.* **2019**, *91*, 3845-3851.
(2) Weber, M.; Wolf, J.-C.; Haisch, C. Effect of Dopants and Gas-Phase Composition on Ionization Behavior and Efficiency in Dielectric Barrier Discharge Ionization. *J. Am. Soc. Mass Spectrom.* **2023**, *34*, 538-549.
(3) Wolf, J.-C.; Gyr, L.; Mirabelli, M. F.; Schaer, M.; Siegenthaler, P.; Zenobi, R. A Radical-Mediated Pathway for the Formation of [M + H]+ in Dielectric Barrier Discharge Ionization. **2016**, *27*, 1468-1475.
(4) Riva, M.; Pospisilova, V.; Frege, C.; Perrier, S.; Bansal, P.; Jorga, S.; Sturm, P.; Thornton, J.; Rohner, U.; Lopez-Hilfiker, F. Evaluation of a reduced pressure chemical ion reactor utilizing adduct ionization for the detection of gaseous organic and inorganic species. *Atmos. Meas. Tech.* **2024**, *17*, 5887-5901.